ORIGINAL ARTICLE

Application of uncertain models of sliding zone on stability analysis for reservoir landslide considering the uncertainty of shear strength parameters

Yang Xue[1,2] · Fasheng Miao[1] · Yiping Wu[1,2] · Linwei Li[1] · Jiajia Meng[1]

Abstract

The shear strength parameters (SSPs) of slip soil, which control the stability and evolution process of a landslide, exist some uncertainty that should be characterized and considered significantly in the stability analysis. In this paper, a typical reservoir landslide with double-sliding zones is taken as a case study. The statistical characteristics of SSPs in sliding zones are first analyzed using the geostatistical method and the Copula method, especially the spatial variation features, scales of fluctuation, and correlation of SSPs. Then, random variable models for the shallow sliding zone and nonstationary random field models with various vertical scales of fluctuation for the deep sliding zone are established separately. Finally, by employing the nonintrusive stochastic finite element program, the fluid–solid numerical simulation of a real hydrological year is carried out to obtain the landslide displacement, element failure probability, and factor of safety. The results demonstrate that incorporating spatial variability into the SSPs of slip soil led to a fundamental change in landslide stability and deformation. Our study provides some references for the reliability assessment of reservoir landslides considering the uncertainties and the spatial variation characteristics of SSP in the sliding zone.

Keywords Reservoir landslide stability · Double-sliding zones · Shear strength parameters · Spatial variability · Nonintrusive stochastic finite element simulation

1 Introduction

Reservoir landslide is a common type of geological hazard in the Three Gorges Reservoir Area (TGRA) and causes serious economic losses and casualties [1]. The deformation and stability analysis of reservoir landslides are very important for the prevention and mitigation of disaster. The sliding zone is a critical structure that controls the evolution process and deformation characteristics of a landslide and is the result of the differential movement of the sliding mass [2, 3]. For the slip soil which goes through the process from the original weak rock layer to the shear rupture zone, the physical and mechanical properties, especially the SSPs, are critical for landslide stability analysis and landslide prevention.

With regard to the reservoir landslide, some tests and measurements, such as the geological investigation [3, 4], laboratory test [5–8], in situ experimental station [3, 9], and structural observation [10, 11], have been carried out to explore property characteristics of slip soil. Several research results show that the microstructure, material composition, particle-size distribution, and SSPs in various spatial positions of the sliding zone varied significantly [8, 12]. And the SSPs are related to the material composition, particle-size distribution, water content, microstructure, and stress distribution. The spatial variability of SSPs exists objectively in the sliding zones. The random deposition, geological movement, hydrogeological environment, and stress distribution are the reason for the spatial variability of property characteristics [13, 14]. When considering the significance of the SSPs in the sliding zone to the stability and evolution process of landslides, it is necessary to investigate the effect of the spatial variability on the reservoir landslide stability.

✉ Yiping Wu
wyp892@126.com

1 Faculty of Engineering, China University of Geosciences, No. 388 Lumo Road, Wuhan 430074, People's Republic of China

2 Research Center of Geohazard Monitoring and Warning in the Three Gorges Reservoir, Wanzhou, Chongqing 404000, People's Republic of China

With the development of the reliability method [15–17], random field method [18–22], and Bayesian method [23–25], the uncertainty and spatial variability of soil properties have been widely studied in slope or landslide engineering. The random variable (RV) model and spatial variation model are usually established to characterize the variability of soil properties. In addition, the effects of variability of soil properties on slope stability are generally explored. However, for the spatial variability of SSPs, many scholars focus on the simple slope by building the stationary random field model [18, 20] and the nonstationary random field (NSRF) model [19, 21]. There are few researches on the spatial variability of SSPs of reservoir landslide, especially the sliding zone. Most research concerning the variability of SSPs of slip zone soil is currently focused on RV models [26, 27], which could not consider the inherent spatial variability. The difficulties and economic costs of excavating and sampling in landslide investigations may be the main reason to hinder the application of spatial variability.

The characterization of the correlation between cohesion (c) and friction angle (φ) plays an important role in the establishment of uncertain models. It has significant effects on the stability analyses of a landslide. At present, the c and φ are usually treated as independent random variables [19, 21], and same distribution types (e.g., normal distribution, lognormal distribution) to simplify the calculation. However, in geotechnical engineering, the negative correlation between c and φ exists in some rock and soil mass [12, 28], and there are many correlation structures for the SSPs, not only the Gaussian [29]. The Copula method, which can identify the optimal correlation structures of c and φ, provides a general and flexible way for constructing the joint probability distribution of multivariate data. Using this method, the negative correlation of c and φ can be well considered in the uncertain models.

Huangtupo No. 1 riverside sliding mass (No. 1 landslide) is the sublandslide of the Huangtupo landslide [3–5, 8–10], which is the largest reservoir landslide in TGRA. Multistage geological investigations and a large in situ experimental station have been applied to the No. 1 landslide. Researches on the sliding zone of No. 1 landslide, including the evolution characteristics [3], macro-and micro-structural behavior [7, 8, 10], creep properties [30], shear strength [8, 9, 30, 31], and deformational characteristics [3, 4, 31], have been extensively investigated. These studies show that the spatial variability of the sliding zone exists objectively in the No. 1 landslide. In addition, a preliminary study of the spatial variability of the sliding zone based on the laboratory test and fractal dimension has been explored by Lu et al. [8]. However, for the consideration of the spatial variability of SSPs, there is no research on the deformation and stability analysis of the No. 1 landslide.

This paper presents a framework for uncertain model construction of sliding zone and stability analysis of reservoir landslide. A series of analyses and comparisons are performed to explore the effect of SSPs uncertainty of slip soil on the No. 1 landslide stability. First, statistical characteristics, spatial trend characteristics, and scales of fluctuation (SOFs) are analyzed and evaluated for the SSPs in sliding zones. Secondly, the construction processes of sliding zone models are designed with the consideration of the uncertainty and the correlation of SSPs. On this basis, a nonintrusive numerical simulation program about the model database input and database output is provided. The numerical simulation of uncertain models is carried out under a hydrological year condition. Finally, parameter variation characteristics, landslide surface displacements, factor of safety (FS), and element failure probabilities (EFPs) are explored for various uncertain models. A few concluding remarks are presented.

2 Methodology

2.1 Copula method

Copulas are multivariate distribution functions that couple a multivariate distribution to its one-dimensional marginal distribution. According to Sklar's theorem, a bivariate distribution, $F(c, \varphi)$, can be expressed in terms of a Copula function $C(u_1, u_2; \theta)$.

$$F(c, \varphi) = C[F_1(c), F_1(\varphi); \theta] = C(u_1, u_2; \theta), \qquad (1)$$

where θ is a Copula parameter describing the dependence between c and φ, it can be calculated from the Kendall rank correlation coefficient τ determined by the Eq. (2). The marginal distributions $u_1 = F_1(c)$ and $u_2 = F_2(\varphi)$.

$$\tau = 4 \int_0^1 \int_0^1 C(u_1, u_2; \theta) dC(u_1, u_2; \theta) - 1. \qquad (2)$$

From Eq. (1), the bivariate probability density function $f(c, \varphi)$ of c and φ can be obtained as

$$f(c, \varphi) = D(u_1, u_2; \theta) f_1(c) f_2(\varphi), \qquad (3)$$

where $D(u_1, u_2; \theta) = \partial^2 C(u_1, u_2; \theta) / \partial u_1 \partial u_2$ is a Copula density function, $f_1(c)$ and $f_2(\varphi)$ is the marginal density functions of c and φ. The best-fit Copula can be identified by using the Akaike Information Criterion (AIC) and the Bayesian Information Criterion (BIC) [28, 29]. A Copula corresponding to the smallest AIC value and BIC value is the best-fit Copula.

2.2 Random field method

According to the spatial variation characteristics of rock and soil structures and properties, the rock and soil properties x_i, at any location i, can be divided conveniently into a deterministic trend component t_i and a residual component ε_i as follows [13]:

$$x_i = t_i + \varepsilon_i. \tag{4}$$

An NSRF model needs to be established once the trend component t_i changes obviously with locations i[19, 21]. It is related to the loading history and depositional conditions. After the trend component is removed, the residual component ε_i can be characterized by a probability density function with zero mean and standard deviation SD_ε. And the SD_ε can be evaluated as

$$SD_\varepsilon = \sqrt{\frac{1}{n-1} \sum_{i=1}^{n} (\varepsilon_i)^2}, \tag{5}$$

where n is the number of data points [14].

In this study, considering the change of the trend component along the horizontal direction, a 2D NSRF model of c and φ in the deep sliding zone is built. According to formula (4), the spatial variability of soil properties $H^{c,\varphi}(x, y)$ can be described by

$$H^{c,\varphi}(x, y) = H_0^{c,\varphi}(x, y) + b^{c,\varphi}(x)x, \tag{6}$$

where x, y are the coordinates in the 2-D domain. $H_0^{c,\varphi}(x, y)$ is a stationary random field with the mean $u_{H_0^{c,\varphi}}$ and the standard deviation $\vartheta_{H_0^{c,\varphi}}$ of c and φ. $b^{c,\varphi}(x)$ is a deterministic trend function regard to the distance x. Among them, the $\vartheta_{H_0^{c,\varphi}}$ is equal to the standard deviation SD_ε of the residual component, the $u_{H_0^{c,\varphi}}$ and the $b^{c,\varphi}(x)$ can be determined by fitting the trend component.

The midpoint method is employed to discretize the stationary random field $H_0^{c,\varphi}(x, y)$, because of its construct conveniently and function effectively [21]. During the calculation process, some common autocorrelation functions can calculate the correlation coefficient $\rho(\tau_x, \tau_y)$ of soil properties at the centroids of elements. Taking the Gaussian autocorrelation function as an example, $\rho(\tau_x, \tau_y)$ can be characterized by:

$$\rho(\tau_x, \tau_y) = \exp\left(-\pi\left(\frac{\tau_x^2}{\delta_h^2} + \frac{\tau_y^2}{\delta_v^2}\right)\right), \tag{7}$$

where τ_x, τ_y are the horizontal and vertical absolute distances, respectively, and δ_h, δ_v are the horizontal and vertical SOFs, respectively.

Autocorrelation distance (or SOF) is used to describe the spatial extent within which soil properties show a significant correlation [32]. In order to assess the SOF, the autocorrelation function (ACF) method [33] is adopted in this paper. By fitting the sample ACF data curves with different analytical ACF models, the optimal analytical ACF model can be determined, and the analytical ACF model parameter is the autocorrelation distance.

2.3 Construction procedures for uncertain models

In order to explore the effect of the randomness and spatial variability of SSPs on the stability of the No. 1 landslide, the NSRF model of the deep sliding zone and the RV model of the shallow sliding zone are constructed separately in this study. And due to the randomness and the spatial variability of input parameters, the finite element software needs to run many times. Some input parameters in study regions are different for different elements. Therefore, we developed an interface for ABAQUS software using MATLAB software. The basic implementation procedures, as can be observed in Fig. 1, are as follows:

(1) Generate the independent standard normal distribution variable ξ by using the Latin hypercube sampling technique. $\xi = [\xi_c, \xi_\varphi]^T = \left[\xi_c = (\xi_{c,1}, \xi_{c,2}, \cdots, \xi_{c,n})^T, \xi_\varphi = (\xi_{\varphi,1}, \xi_{\varphi,2}, \cdots, \xi_{\varphi,n})^T\right]$. Where n is the number of elements of the sliding zone.

(2) Identify the optimal Copula function of SSPs data in two sliding zones from Gaussian, Frank, Plackett, and No.16 Copulas with the AIC and BIC criteria.

(3) Obtain the dependent standard uniform variable U from ξ based on the optimal Copula function and the Copula parameter θ.

$$U = \left[U_c, U_\varphi\right]^T = \left[U_c = (U_{c,1}, U_{c,2}, \ldots, U_{c,n})^T,\right.$$
$$\left. U_\varphi = (U_{\varphi,1}, U_{\varphi,2}, \ldots, U_{\varphi,n})^T\right].$$

(4) Based on the above steps, the RV and NSRF models can be obtained using the following steps.

The basic construction step of the RV model is below:

(a) Translate the dependent standard uniform random variable U into the random variable H with the distribution of c and φ based on the equivalent possibility transformation rule.
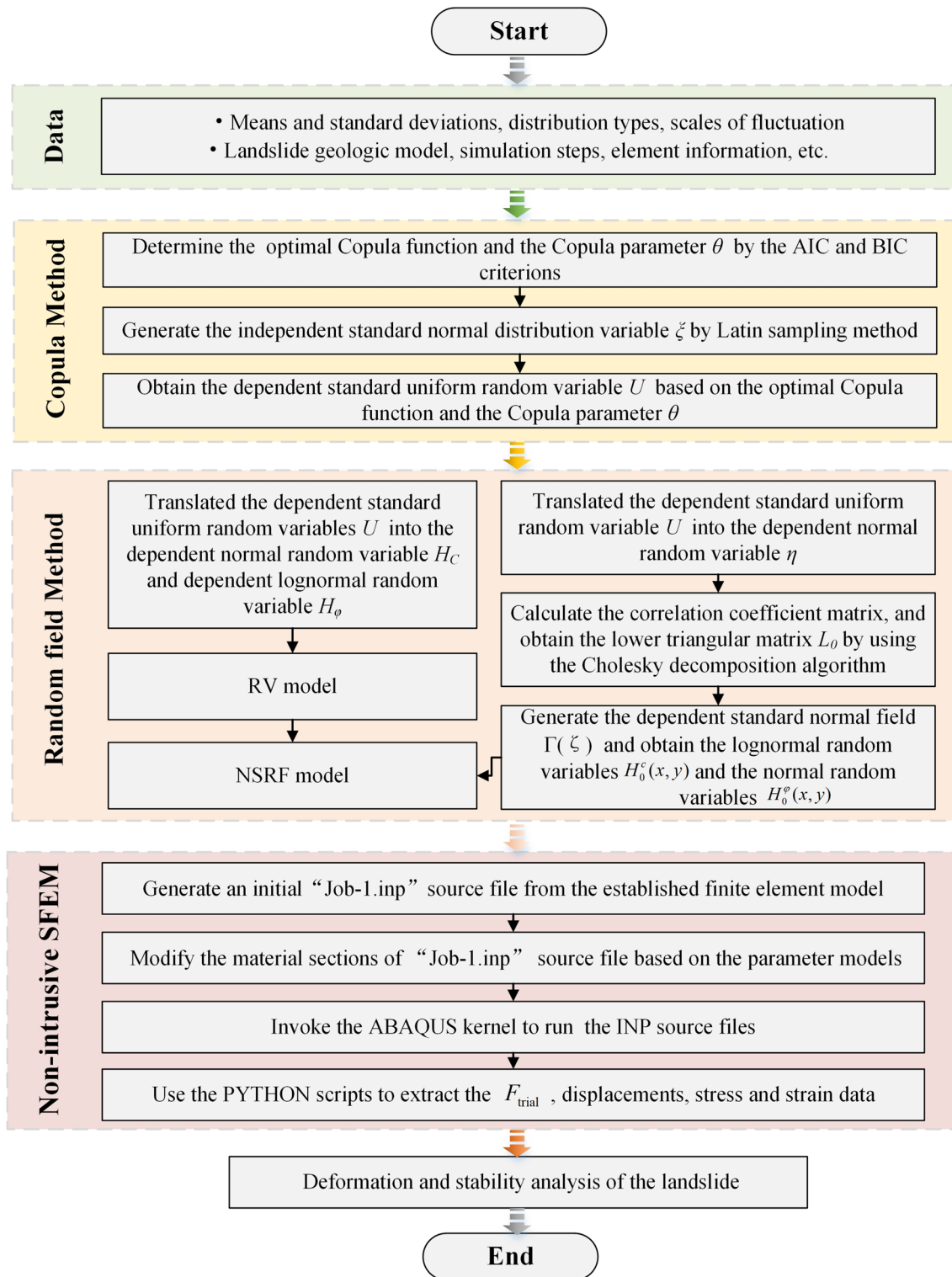
Start

Data
- Means and standard deviations, distribution types, scales of fluctuation
- Landslide geologic model, simulation steps, element information, etc.

Copula Method

Determine the optimal Copula function and the Copula parameter θ by the AIC and BIC criterions

Generate the independent standard normal distribution variable ξ by Latin sampling method

Obtain the dependent standard uniform random variable U based on the optimal Copula function and the Copula parameter θ

Random field Method

Translated the dependent standard uniform random variables U into the dependent normal random variable H_C and dependent lognormal random variable H_φ

RV model

NSRF model

Translated the dependent standard uniform random variable U into the dependent normal random variable η

Calculate the correlation coefficient matrix, and obtain the lower triangular matrix L_0 by using the Cholesky decomposition algorithm

Generate the dependent standard normal field $\Gamma(\varsigma)$ and obtain the lognormal random variables $H_0^c(x,y)$ and the normal random variables $H_0^\varphi(x,y)$

Non-intrusive SFEM

Generate an initial "Job-1.inp" source file from the established finite element model

Modify the material sections of "Job-1.inp" source file based on the parameter models

Invoke the ABAQUS kernel to run the INP source files

Use the PYTHON scripts to extract the F_{trial}, displacements, stress and strain data

Deformation and stability analysis of the landslide

End

Fig. 1 Schematic diagram of the calculation and analysis flow

$$H = \left[H_c, H_\varphi\right]^T = \left[H_c = \left(H_{c,1}, H_{c,2}, \ldots, H_{c,n}\right)^T,\right.$$

$$\left. H_\varphi = \left(H_{\varphi,1}, H_{\varphi,2}, \ldots, H_{\varphi,n}\right)^T\right].$$

The basic construction steps of the NSRF model are below:

(b) Translate the dependent standard uniform random variable U into the dependent normal random variable $\eta = \left[\eta_c, \eta_\varphi\right]^T$.

(c) Calculate the correlation coefficient matrix consisted of correlation coefficients $\rho\left(\tau_x, \tau_y\right)$ between any two elements. And obtain the lower triangular matrix L_0 by factoring the correlation coefficient matrix with the Cholesky decomposition algorithm.

Generate the dependent standard normal random field Γ using the formula $\Gamma = \eta L_0$, and translate the dependent standard normal random field Γ into the real distribution random field of c and φ based on the equivalent possibility transformation rule. By the end

of this step, the stationary random field model $H_0^{c,\varphi}(x, y)$ can be obtained.

Calculate the NSRF model $H^{c,\varphi}(x, y)$ by Eq. (6).

The basic steps of the noninvasive stochastic finite element are described as follows:

(1) Build a 2D landslide finite element model in ABAQUS CAE using Part, Property, Boundary, Load, Step, Mesh, and Job modules. Save the model input database to an initial INP source file (e.g., Job-1.inp). Then, extract the center coordinates of elements in the sliding zone.

(2) Generate input parameters (e.g., c and φ) through the process in Sect. 2.3. Then, modify the material section of the initial INP source file. And generate the complete INP source files.

(3) Call ABAQUS kernel in batch based on the MATLAB platform, the INP source files and user subroutines files (e.g., Job-1.for) can run in a loop. And generate the ODB source files for each Job.
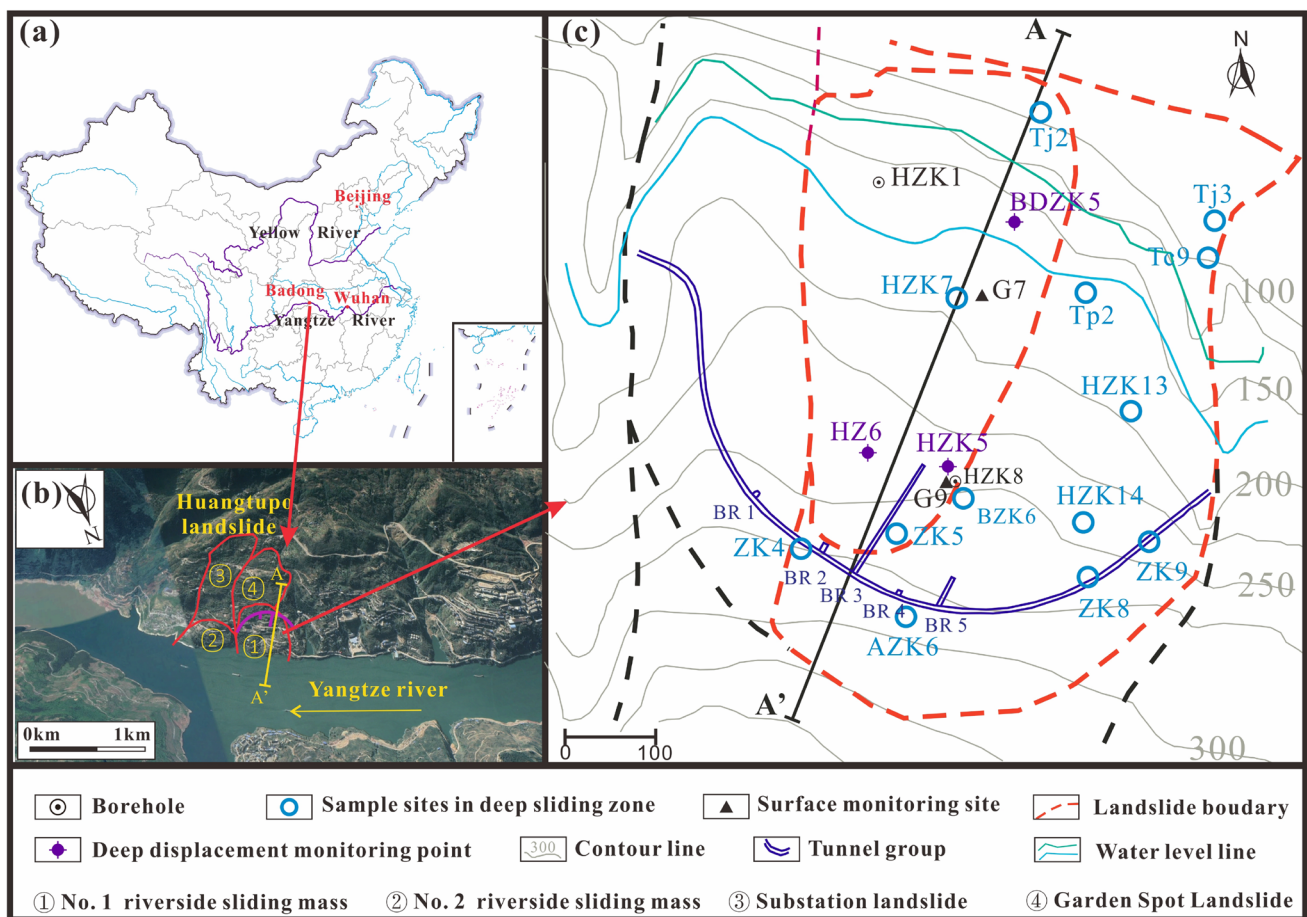

Fig. 2 Location and a plane view of the study area, **a** China, **b** Huangtupo landslide, **c** No. 1 landslide

(4) Call PYTHON scripts based on the MATLAB platform to extract the F_{trial}, displacements, stress, and strain data.

3 Case study

3.1 Study area and data collection

The Huangtupo landslide, located on the south bank of the Yangtze River in the TGRA, is situated in Badong County, Hubei Province, China. As shown in Fig. 2, the Huangtupo landslide is subdivided into four regional landslides, namely, No. 1 riverside sliding mass, No. 2 riverside sliding mass, Garden Spot landslide, and Substation landslide [3–5]. The No. 1 landslide has a length of 770 m from north to south and a width of 480 m from east to west. Current literatures show that the No. 1 landslide has the poorest stability and largest deformation [3]. And the No. 1 landslide composed of two sublandslides underwent at least two movement periods. The formation timing of the shallow sliding zone is about 40 ka or 50 ka (ka stands for a thousand years), the formation timing of the deep sliding zone is approximately 100 ka.

To study the No. 1 landslide geological model with double sliding zones, the cross section A–A´, which has been proved and used by some researchers [31, 34], is selected as the studied profile. As shown in Fig. 3, branch No.3 passes through the two sliding zones with A and B points. Point A is about 23–33 m away from the main tunnel. Point B is about 135–140 m away from the main tunnel. The research results show that the dips and dip directions of sliding zones in the two points are very different [3, 34]. And the two inclinometer profiles of boreholes, HZK5 and BDZK5, are drawn to show the position of significant deformation. It can be seen that two points with depths of 55 m and 76 m have a relatively large displacement in the borehole HZK5. And the borehole BDZK5 shows that locations with depths of 41 m and 63 m have a relatively large displacement. These results imply that the No. 1 landslide has a double-sliding zone in the A–A´ cross section. The investigation data show that the thickness of the deep sliding zone is between 0.2 and 10.0 m, and the thickness of the shallow sliding zone is between 0.2 m and 8.0 m.

In the past years, investigations from the Hubei Survey and Design Institute for Geohazard Engineering [35] and the Three Gorges Research Center for Geohazards of the China University of Geosciences [36] have been carried out
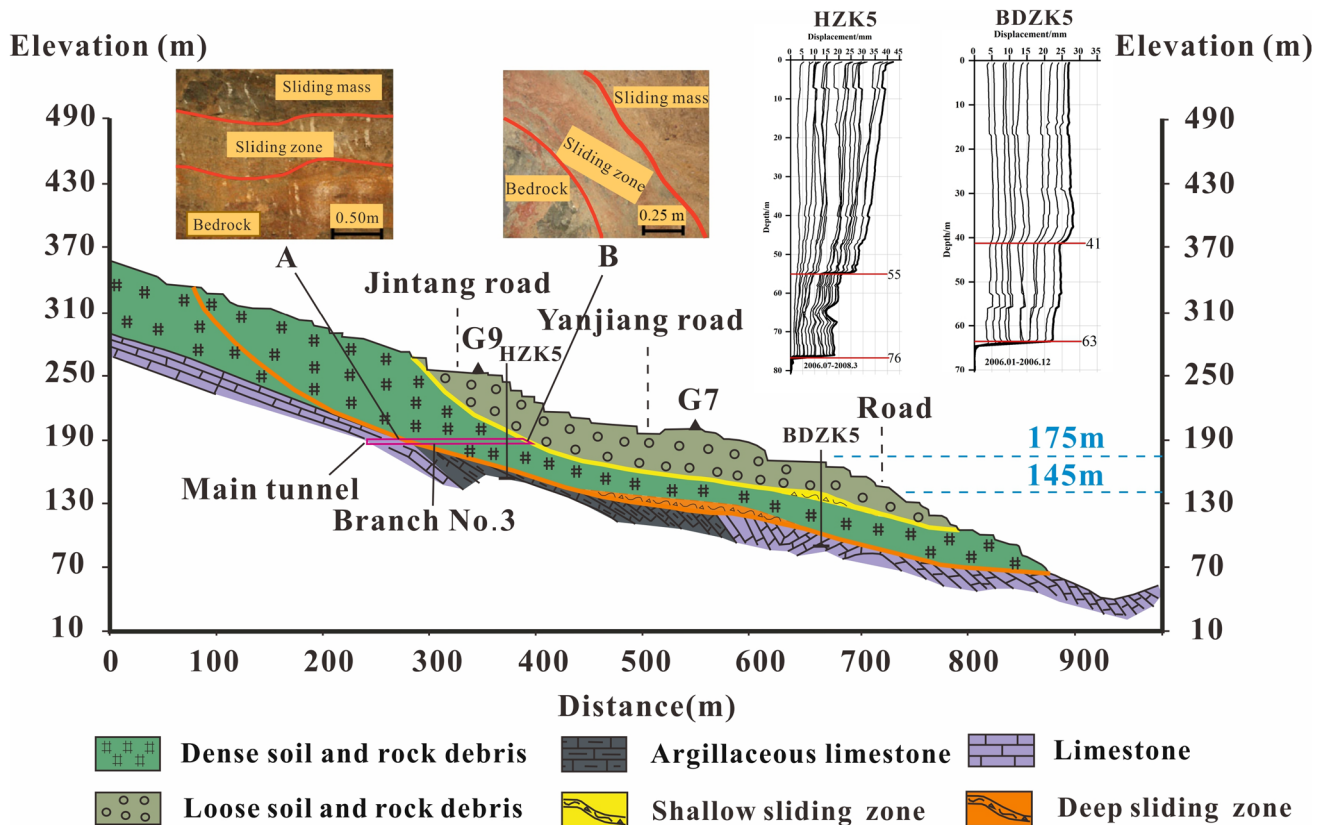

Fig. 3 A–A´ geological profile of the No. 1 landslide

Table 1 Data of SSP in sliding zones

Location	Test sites	c/KPa	φ/°	Test sites	c/KPa	φ/°	Test sites	c/KPa	φ/°
Deep sliding zone	Tj3[HI]	222	15	HZK7[HI]	100	9	HZK13[HI]	80	12
	Tj3[HI]	124	19	HZK7[HI]	70	18	HZK13[HI]	43	12
	Tj2[HI]	128	9	TP2[HI]	94	18	HZK14[HI]	36	8
	Tj2[HI]	170	12	ZK9[HI]	13	26.1	TC9[HI]	88	14
	BZK6[CI]	25	26.3	ZK8[CI]	23	19.3	ZK5[CI]	28	16.7
	AZK6[CI]	10	26.6	ZK4[CI]	23	17.2			
Shallow sliding zone and weak zone	HZK13[HI]	50	15	HZK1[HI]	59	14	HZK8[HI]	15	13
	ZK9[CI]	23	25.1	ZK8[CI]	20	14.4	AZK6[CI]	23	25.1
	ZK9[CI]	10	22.8	ZK8[CI]	23	19.1	AZK6[CI]	10	22.8
	BZK6[CI]	18	17.7	ZK5[CI]	22	18.8	BR3[Hua]	36	15.7
	BZK6[CI]	26	23.7	BR3[Hua]	49	18.8	BR3[Tan]	30.2	14.7
	ZK4[CI]	13	27.2	BR3[Li 2018]	23	19.9	BR3[Tan]	20.2	19.1
	ZK5[CI]	22	17.7	BR3[Li 2018]	18.1	17.5	BR3[Li]	12	26.4

Note: The various corner marks (HI, CI, Li, Hua, Tan, Li 2018) denote data sources from literatures (HIGH [35], CISPD [36], Li et al. [30], Hua, [37], Tan, [9], Li et al. [31]) respectively

(a)　　　　　　　　　　　　　　　　　　　　　(b)
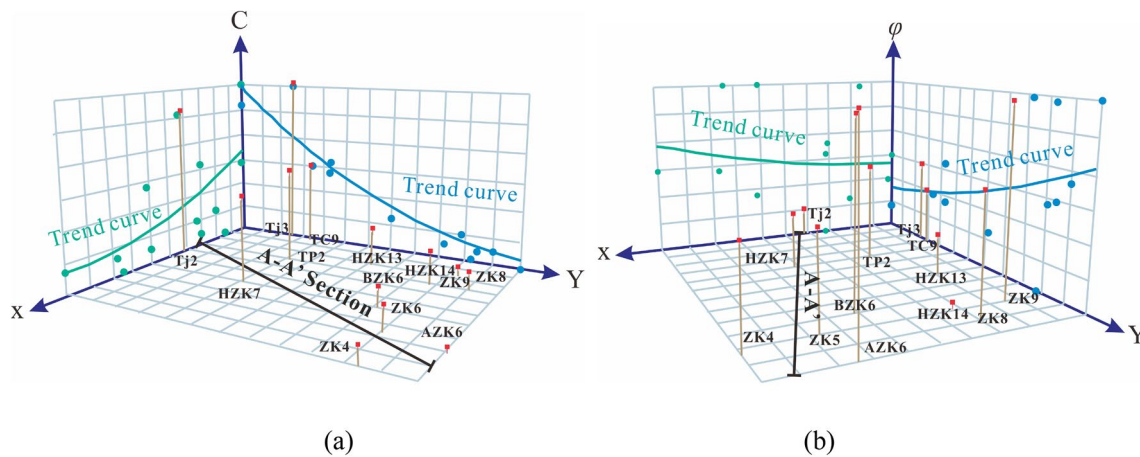
Fig. 4 Plane position and trend variation of SSP in the deep sliding zone, **a** Cohesion. **b** Internal friction angle

in the No. 1 landslide in detail. Some test data of SSPs in double-sliding zones are obtained [9, 30, 31, 35–37]. The data obtained from systematic investigations and laboratory tests are collected in Table 1. The data obtained from direct shear tests or triaxial tests provide valuable information to study spatial variation characteristics of SSPs.

3.2 Statistical analysis

As can be seen from Fig. 2, the collected data are dispersed in the No. 1 landslide, and most sampling points are located in the deep sliding zone. The plane position of data is illustrated in Fig. 4.

In Fig. 4, the x- and y axis represent the plane coordinate. The z axis represents the value of c or φ. There is a clear trend that the c increases along the sliding direction, while

the φ decreases. And the trend can be estimated by a low-order polynomial using the ordinary least squares method. The change of soil materials by location is summarized. At the leading edge of the landslide, the material of the deep sliding zone is silty clay with gravel or breccia, the cohesion ranges from 88 to 222 kPa, and the internal friction angle ranges from 9° to 19°. In the middle part of the landslide, the material of the sliding zone is silty clay with gravel, the cohesion ranges from 43 to 100 kPa, and the internal friction angle ranges from 9° to 18°. At the trailing edge of the landslide, the material of the sliding zone is silty clay with gravel, the cohesion ranges from 10 to 54 kPa, and the internal friction angle ranges from 8° to 26.6°. Taken together, these results suggest that c and φ of the deep slip soil have a regional trend in the sliding direction [8], this trend should be considered to build a geological model of the landslide.

In this paper, the one-sample Kolmogorov–Smirnov test is performed to assess the distribution types of c and φ from the normal and lognormal distributions (see Fig. 5). From the P values of the Kolmogorov–Smirnov test, the optimum probability distribution type of c is the lognormal distribution. However, the hypotheses that the φ comes from the normal and lognormal distributions are not rejected for a significance level of 0.05. Fortunately, thousands of SSPs groups of sliding zone soil in the TGRA are counted by Luo et al. [38] and Li et al. [39]. And research results show that the c and φ variables are supposed to obey the lognormal distribution and the normal distribution, respectively. Therefore, in this study, the lognormal distribution is used for the variable φ. The results obtained from the preliminary statistical analysis of c and φ in the double-sliding zones are presented in Table 2. There is a negative correlation between c and φ, it is consistent with the results reported in geotechnical engineering [28, 29].

In order to build the joint probability distribution of c and φ, the Copulas (e.g., Gaussian, Frank, Plackett, and No.16 Copulas) that allow a wide range of negative correlation coefficients are selected to characterize the dependence [28, 29]. As shown in Table 3, based on the smallest AIC and BIC values, the optimal Copula function of SSPs of the deep sliding zone is the Plackett Copula, and that of the shallow sliding zone is the Gaussian Copula. Based on the best-fit Copula function and the Copula parameter θ, the dependent random variables of c and φ can be generated.

3.3 Determination of the horizontal SOF

According to the distribution characteristics of sampling positions shown in Fig. 2, the locations of some sampling
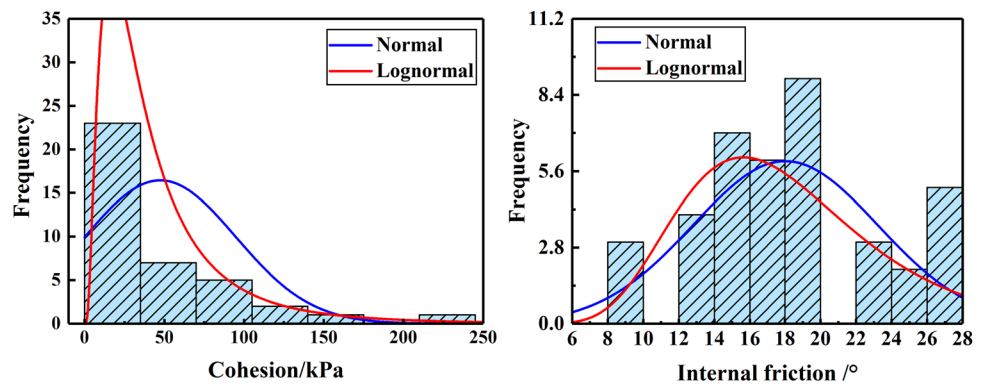
Fig. 5 Histogram of c and φ

Table 2 Statistical values of SSP

	Shear strength	Counter	Mean	Standard deviation	Coefficient of variation	Minimum	Maximum	Spearman correlation coefficient	Distribution type
Deep sliding zone	c	17	75.1	60.1	0.80	10	222	− 0.56	c is logarithm normal and φ is normal
	φ	17	16.3	5.9	0.36	8	26.6		
Shallow sliding zone	c	21	24.9	13.3	0.54	10	59	− 0.34	
	φ	21	19.4	4.3	0.22	13	27.2		
Sliding zone	c	38	47.3	47.9	1.01	10	222	− 0.61	
	φ	38	18.1	5.3	0.29	8	27.2		

Table 3 AIC and BIC values of four Copulas

Data type	Gaussian Copula [θ, AIC, BIC]	Plackett Copula [θ, AIC, BIC]	Frank Copula [θ, AIC, BIC]	No.16 Copula [θ, AIC, BIC]
Deep sliding zone	–, − 5.3246, − 4.4342	**0.1566, − 5.6720, − 4.7817**	–, − 5.1864, − 4.2960	–, − 3.6653, − 2.7749
Shallow sliding zone	**− 0.3404, − 1.0112, 0.0334**	–, − 0.7587, 0.2859	–, − 0.7032, 0.3413	–, − 0.8393, 0.2052

Bold values indicate the minimum value of the AIC and BIC values

points in the shallow sliding zone are relatively concentrated. It is unrealistic to obtain the spatial variation characteristics of SSPs of the shallow slip soil. Therefore, the deep sliding zone is presented as the primary example to obtain the SOF. In addition, there is no sufficient data to calculate the vertical SOF, because some sampling elevations are not accurate, and the sampling points are relatively concentrated in the vertical direction. Fortunately, it is more rational for the longitudinal section A–A´ used in this study to calculate the horizontal SOF. And the vertical SOFs are assumed to be 0.25, 0.5, 0.75, and 1.0 times of the horizontal SOF.

In order to obtain the horizontal SOF, which need uniformly distributed sample sites and much data [33], some interpolation methods [32], which can consider the spatial correlation of the original data, should be chosen to obtain a reliable estimate of the missing data at locations where it should have been measured in the profile A–A'. Because of the robustness of Kriging, even with a naive selection of parameters, the method will do no worse than the conventional spatial interpolation method [40]. And many researches have demonstrated that Kriging is a better interpolation method with high accuracy and low bias. The universal Kriging method, which can consider the variation tendency of data [41], is adopted in this paper.

ArcGIS software has powerful geostatistical analysis functions, and the universal Kriging method can be easily applied in ArcGIS 10.1. In this study, the universal Kriging interpolation is carried out using the interpolation tools available in the ArcGIS 10.1 geostatistical analyst module. The basic step is described in detail in the ESRI ArcGIS resource center. During the interpolation process, the trend is removed using the polynomial fitting tool, the order of the polynomial is set 2, and the exponential function is selected as the kernel function and the semi-variogram. Log transformation is used for the variable c, and leave the default settings. The interpolation results of c and φ are shown in Fig. 6.

From the trailing edge to the front edge of No.1 landslide, sixty data points are uniformly distributed in section A–A´. The c and φ values with the distance are plotted in Fig. 7. As can be observed, there is an increasing trend in Fig. 7 (a) and a decreasing trend in Fig. 7b. And trend removal by least squares regression has been utilized. The stationary residuals are drawn separately in Fig. 7 c,), then the standard deviation SD_ε of c and φ are calculated using the Eq. (5).

The sample ACF of the stationary residuals is firstly calculated. Then, the single exponential and Gaussian models, which are two commonly used analytical ACF models, are used to fit the sample ACF. The ACF fitting curves are drawn in Fig. 7e, f, and the fitting results are tabulated in Table 4. It can be noted that the more suitable model is the Gaussian model with a higher coefficient of determination. The horizontal SOFs of c and φ are 38.4 m and 54.1 m, respectively. The autocorrelation distance reported by El-Ramly et al. [13] in the horizontal varies between $10\sqrt{\pi}$ m and $40\sqrt{\pi}$ m. The average of c and φ horizontal SOFs is used to establish random field models.

3.4 Numerical simulation

The finite element model of the A–A´ section is built as shown in Fig. 8. The landslide model is divided into 2301 linear quadrilateral elements of type CPE4RP, coupling the pore pressure and the displacement. The linear quadrilateral element can meet the requirement of displacement accuracy and has low computational cost. The shallow sliding zone has 107 elements, and the deep sliding zone has 256 elements. The ideal elastic–plastic and Mohr–Coulomb failure criteria are adopted. And the bottom displacements of the model in vertical and horizontal directions are restrained. The deep sliding surface is considered an impervious boundary. The landslide surface below the reservoir water level is set to the pore pressure and pressure boundaries. The
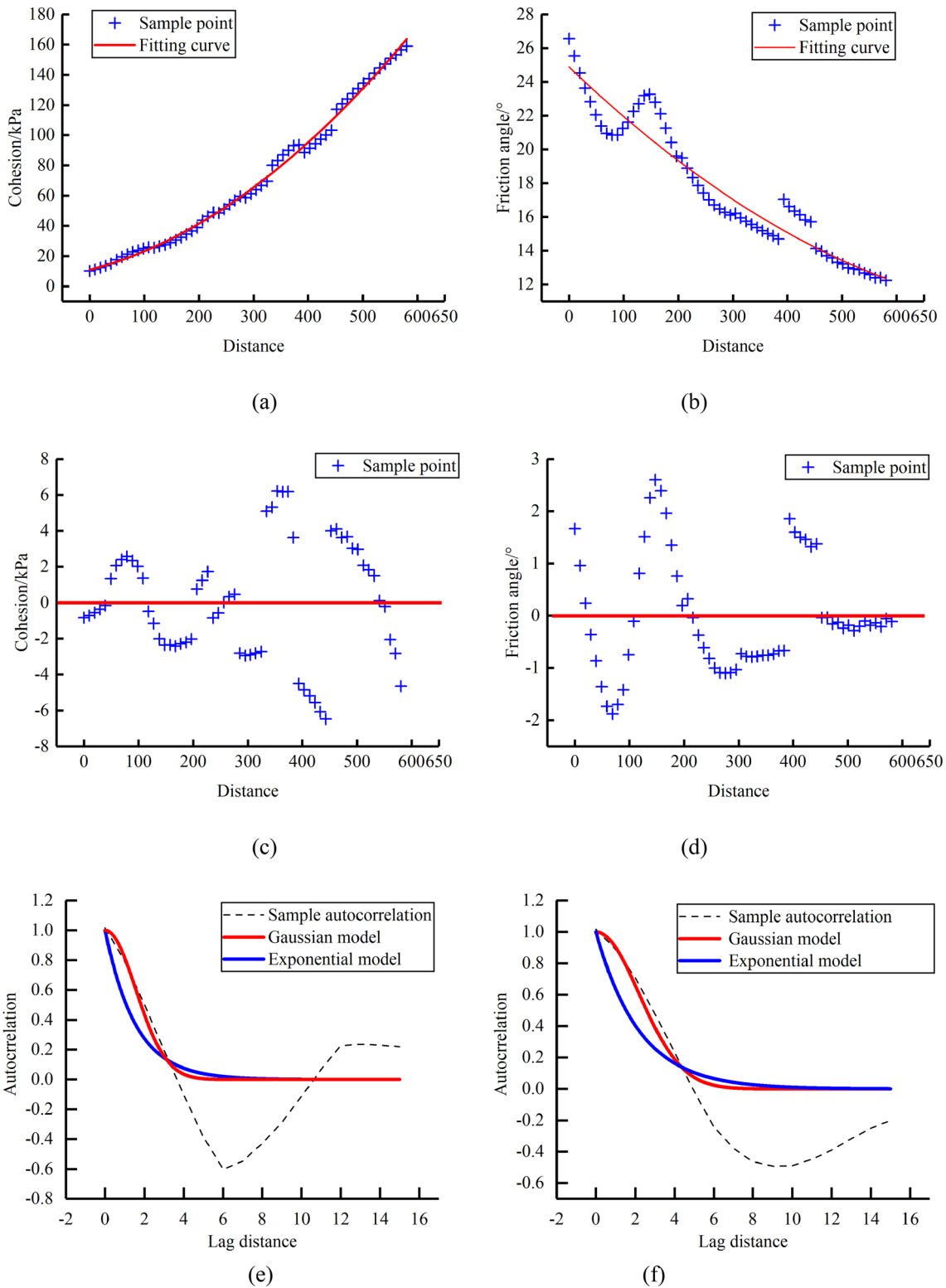
Fig. 6 Interpolation results of c and φ

Legend
Value
High : 167.3
Low : 11.5

(1) c

Legend
Value
High : 19.7
Low : 14.7

(2) φ
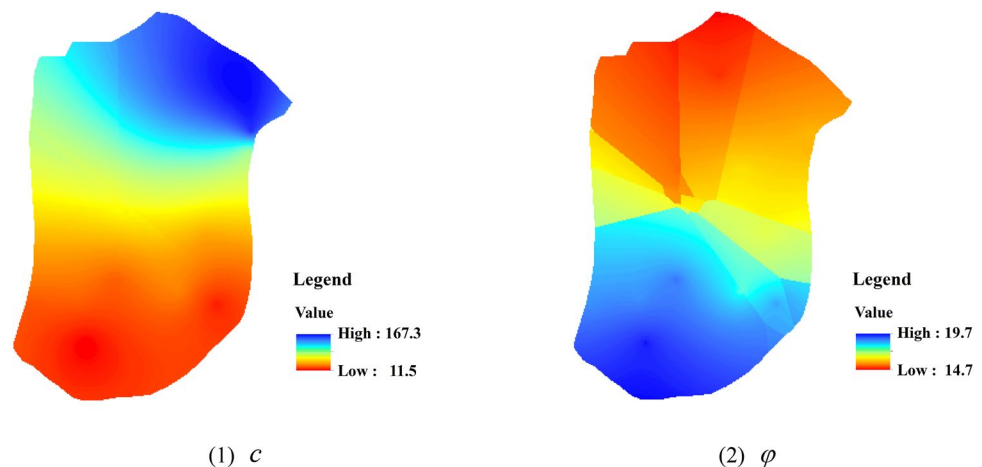
Fig. 7 **a**, **b** Are the estimated data of c and φ. **c**, **d** Are the stationary residuals of c and φ. **e**, **f** Are the ACF fitting curves of c and φ

Table 4 Fitting results of SOFs

Data type	Trend function	SD_ε	SOF	ACF models	Coefficient of determination
c	$f_c(x) = 10.84 - 0.095x + (2.9E-4)x^2$	3.19	**38.4**	**Gaussian**	**0.582**
			30.5	Exponential	0.519
c	$f_\varphi(x) = 24.8 - 0.031x + (1.62E-5)x^2$	1.10	**54.1**	**Gaussian**	**0.631**
			45.1	Exponential	0.552

Bold values indicate a higher coefficient of determination
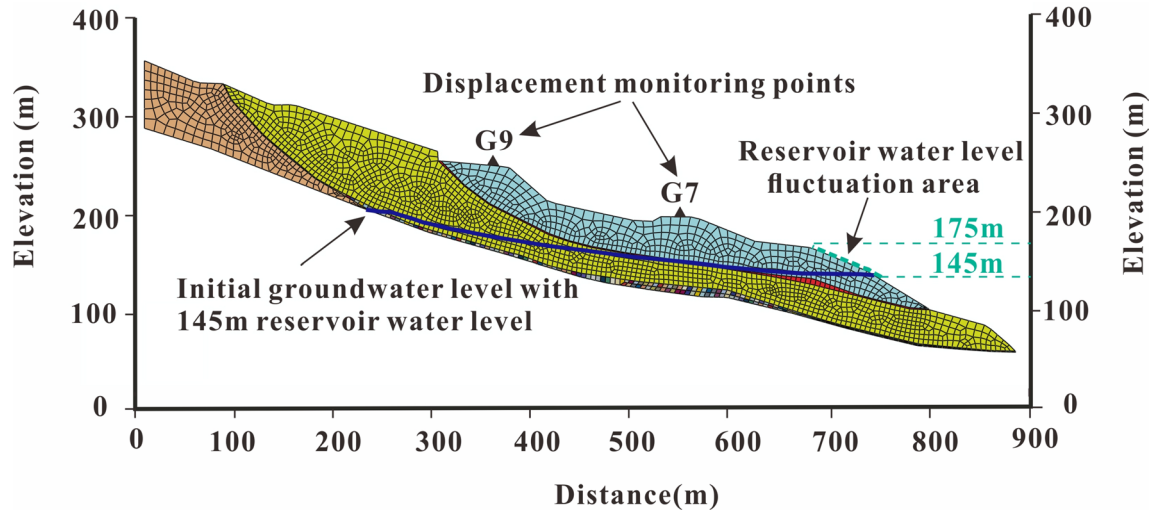
Fig. 8 Finite element model of section A–A´ of the No.1 landslide

Table 5 Physical and mechanics parameters of materials [34]

Medium	Unit weight (KN/m³)	Elasticity modulus (MPa)	Poisson ratio	Cohesion (KPa)	Internal friction angle (°)	Saturated hydraulic conductivity (m/d)	Void ratio
Shallow sliding mass	21.0	727.0	0.31	80	25	2.35	0.28
Deep sliding mass	23.0	2178.0	0.29	190	34	1.88	0.25
Shallow sliding zone	19.9	28.6	0.34	–	–	0.76	0.24
Deep sliding zone	21.3	36.8	0.35	–	–	0.24	0.23

landslide surface above the water level is the free overflow boundary or rainfall boundary.

Based on the statistical parameters shown in Table 2 and the construction procedures described in the 2.3 section, the SSPs of the shallow sliding zone are generated using the RV model. And the SSPs of the deep sliding zone are generated using the NSRF model. Different vertical SOFs (e.g., 0.25 δ_h, 0.50 δ_h, 0.75 δ_h, 1.00 δ_h, $\delta_h\delta_h$ is the horizontal SOF) are used to establish various NSRF models. In addition to the SSPs of sliding zones, the Van Genuchten soil–water characteristic curve (SWCC) is adopted to solve the seepage governing equation. The SWCC fitting parameters (e.g., 0.233, 1.255) of a typical reservoir landslide [42] in TGRA are adopted. Other material parameters are presented in Table 5.

In this article, the strength reduction with the finite element (SRFE) method [42–45] is adopted to determine the FS with the numerical nonconvergence criterion. The two sliding zones are selected as the strength reduction area to calculate the FSs of the whole No.1 landslide. And the FSs of various uncertain models in different time points are obtained using the ABAQUS restart analysis based on the local SRFE method. And the EFPs of various uncertain models in different time points are also obtained by using the element failure probability method [42].
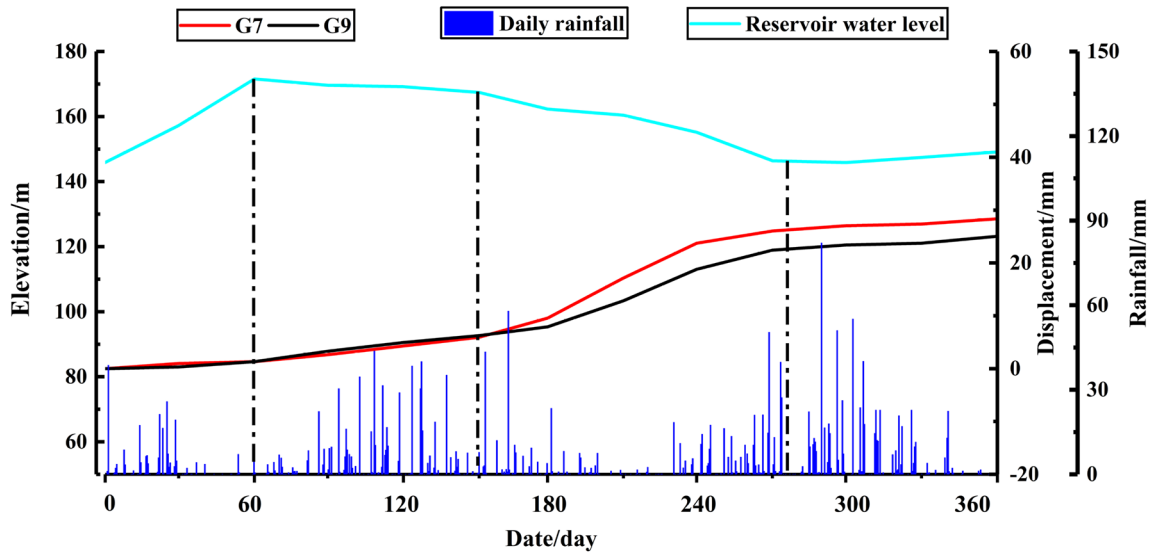
Fig. 9 Monitoring data of the rainfall, reservoir water level, and GPS displacement in 1 year

3.5 Simulation scheme

According to monitoring data of meteorological and hydrological, the daily rainfall and reservoir water level of one hydrological year are shown in Fig. 9. The real daily rainfall condition is adopted, and we simplified the simulation condition of the reservoir water as follows:

Step 1. From 145 to 175 m, lasting 60 days, rising stage of reservoir water;

Step 2. At 175 m reservoir water level, lasting 60 days, stable stage of reservoir water;

Step 3. From 175 to 145 m, lasting 160 days, drawdown stage of reservoir water;

Step 4. At 145 m reservoir water level, lasting 80 days, stable stage of reservoir water.

According to the annual monitoring data of groundwater level in borehole ZK4, the groundwater level is maintained at 210 m throughout the year [34]. On this basis, the initial groundwater level is determined by the steady seepage analysis in ABAQUS.

According to the deformation characteristics of the Huangtupo landslide [3, 34], the No.1 landslide is stable under this simulation condition. However, the
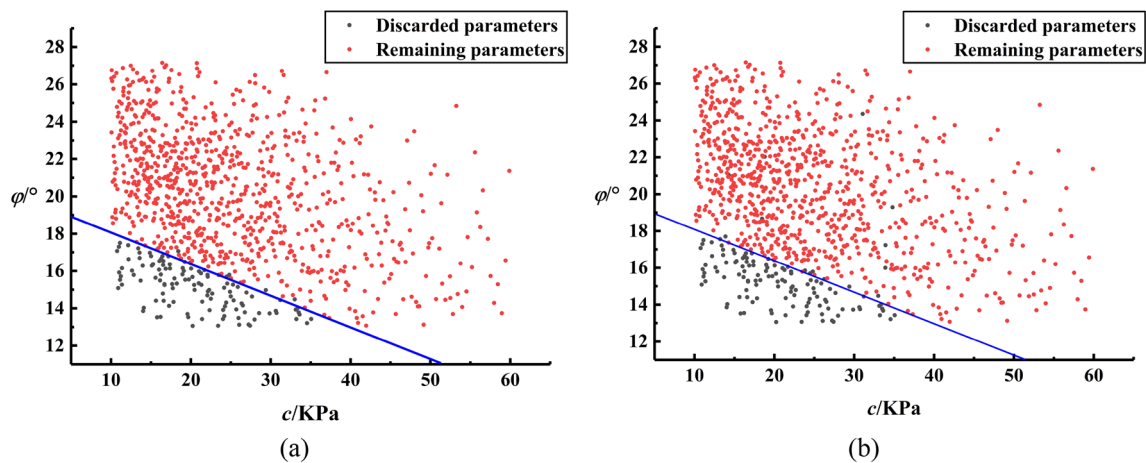
Fig. 10 SSPs in the shallow sliding zone for different NSRF models **a** 0.25 δ_h, **b** 1.0 δ_h

un-convergence problem may occur during the finite element calculation, once c and φ values in double sliding zones deviate from the actual situation. Certainly, other causes of un-convergence need be first excluded roughly. On this basis, we can use the above mechanism, which is a form of back analysis for parameters based on the landslide stability, to eliminate some unreasonable parameters of c and φ in double sliding zones. In this study, 1 000 realizations for uncertain models are carried out. The variation characteristics of c and φ are firstly analyzed. And then the landslide surface displacements, EFPs, and FSs are explored for different uncertain models.

4 Results

4.1 Parameter variation characteristics

Based on the convergence condition of 1000 numerical simulations, the variation characteristics of SSPs of double sliding zones are analyzed. For the SSPs of the shallow sliding zone, 1 000 realizations of c and φ are plotted in Fig. 10. The black dots represent the discarded parameters, while the red dots represent the remaining parameters, and the dark blue line is the dividing line. As can be seen from Fig. 10, there is a boundary between the discarded parameters and the remaining parameters. The region boundary is relatively straight due to the negative correlation of c and φ. The differences of SOF for two NSRF models have little influence on the dividing line by comparing Fig. 10a. b. The region of discarded parameters can be defined by $\varphi = -0.37c + 19$, where $c < 52$ and $\varphi < 19$. In this region, the mean of c and φ are 20.66 kPa and 15.17°, respectively. Under the combination parameters of c and φ over this region, the numerical

simulation process is interrupted. The SSPs of the shallow sliding zone are not reasonable for the No.1 landslide.

For the purpose of studying variation characteristics of the SSPs of the deep sliding zone, the mean, maximum, and minimum of SSPs in the deep sliding zone are used to characterize the parameter variation in one realization. The statistical values of 1000 realizations are plotted in Fig. 11. It is apparent from this figure that no significant differences are found between the mean of the discarded parameters and the mean of the remaining parameters. The maximum and minimum of discarded parameters are within the ranges of the maximum and minimum of remaining parameters, and their differences are almost insignificant. As shown in Fig. 11a, b, the change of SOF also has little effect on the parameter selection. Remarkably, the trend of statistics may result from the constant negative correlation of c and φ.

Overall, the variations of SSPs in the shallow sliding zone are apparent, while those in the deep sliding zone have no obvious regularity. It indicates that the SSPs in the shallow sliding zone have more influence on landslide stability. And the change of NSRF models with different SOFs has a minor effect on the SSPs variation of double-sliding zones. The influences of various SOFs are analyzed and discussed in the discussion section. The remaining parameters are used for subsequent analysis.

4.2 Displacements analysis

In this section, GPS monitoring points (e.g., G7 and G9) and corresponding points in simulation are used to investigate the effect of SSPs uncertainty on the landslide surface displacement. The uncertain model with 0.25 δ_h is taken as a case. The G7 and G9 surface displacement curves are drawn in Fig. 12. It can be observed that the light red and
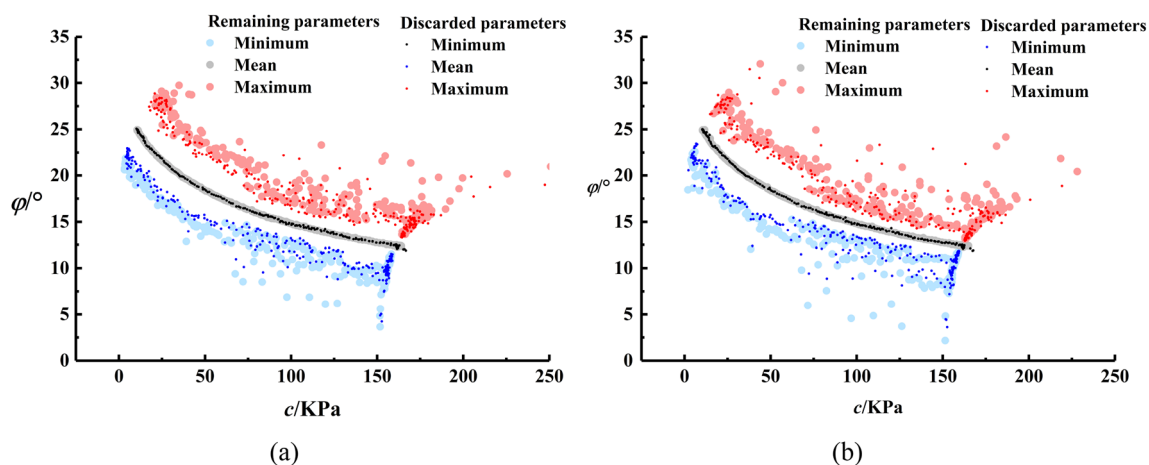

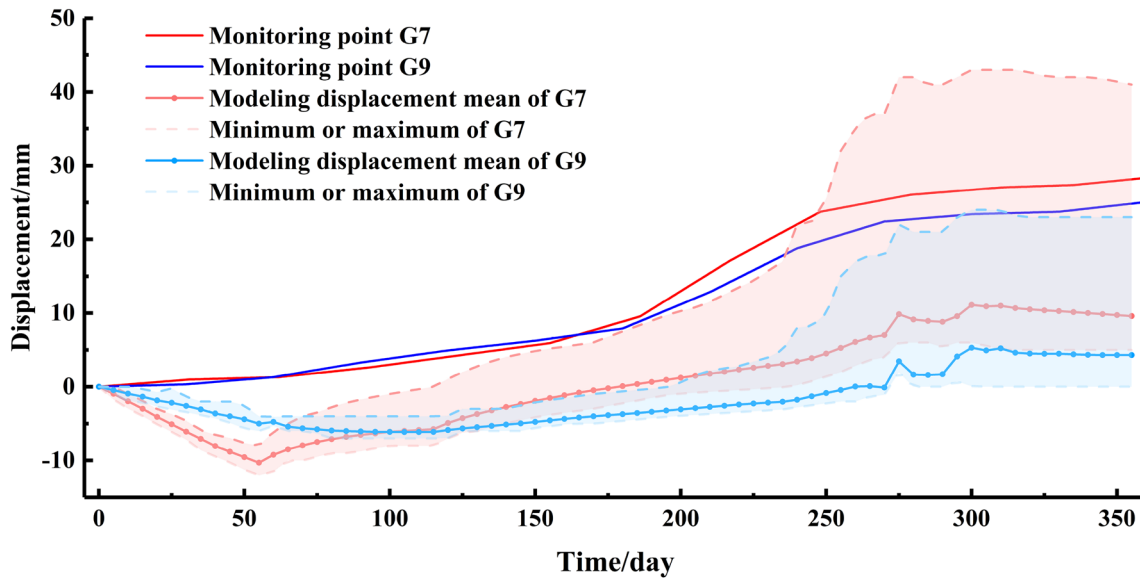**Fig. 11** SSPs in the deep sliding zone for different NSRF models **a** 0.25 δ_h, **b** 1.0 δ_h

Fig. 12 Landslide surface displacement in 1 year for the NSRF model with 0.25 δ_h
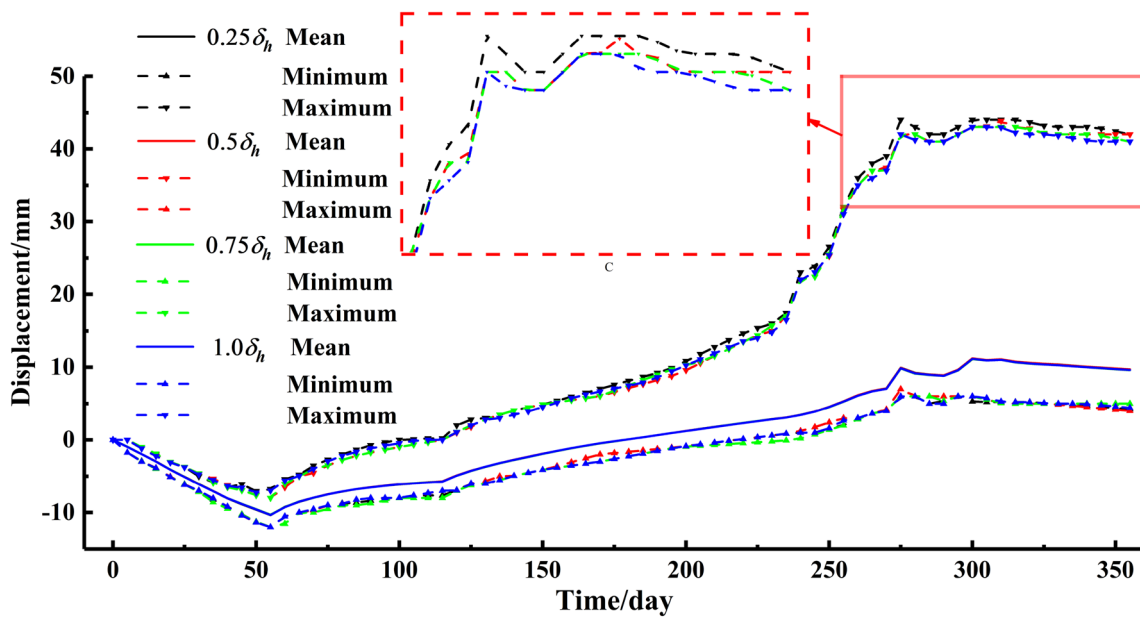

Fig. 13 Landslide surface displacement of G7 in 1 year for NSRF models with different δ_h

light blue areas are the fluctuating ranges of G7 and G9 displacements, respectively, and their mean displacement curves are undoubtedly in these intervals. It can also be noted that the mean displacement curves are not in the middle of their intervals. According to the displacement curves, the deformation of the No. 1 landslide mainly occurs during the decline of reservoir water level (120–280d). The displacement of G7 in the middle-front region is larger than that of G9 in the back part. And it can be seen from Fig. 9 that the rainfall is relatively high in this period.

As can be seen from Fig. 12, for the actual monitoring and modeling displacement curves, the trend of displacement curves is similar, but displacement values are different. More obviously, G7 and G9 points have a displacement trend towards the interior of the landslide for modeling displacement curves from 0 to 60 days, and the period is the rising stage of reservoir water. It can be interpreted that the existence of cracks in the landslide provides space for deformation, and the GPS monitoring points cannot obtain the displacement deformation pointed to the inside of the landslide
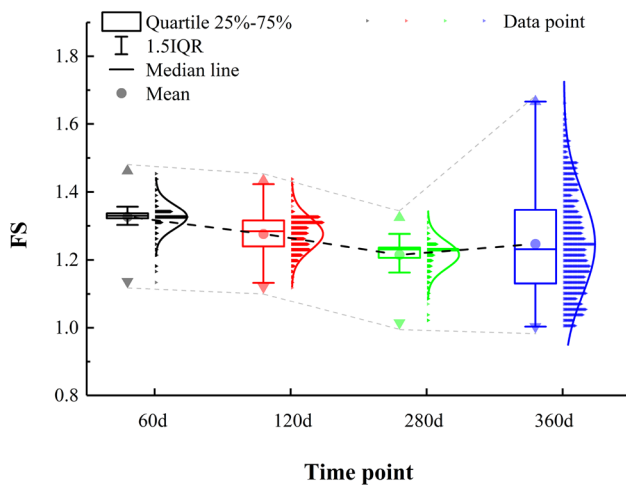
Fig. 14 Boxplot and data distribution of FSs for different time points (NSRF model with 0.25 δ_h)

body [34]. In addition, the material constitutive model and other simulation parameters are also factors affecting modeling displacement.

In order to study the effect of NSRF models with various SOFs on the landslide surface displacement, the mean, maximum, and minimum of G7 displacements with different NSRF models are plotted in Fig. 13. It can be seen that the mean and minimum curves of 0.25 δ_h, 0.5 δ_h, 0.75 δ_h, 1.0 δ_h are basically in coincidence, and there are no meaningful differences. Interestingly, during the period from 270 to 360d, the displacement values of the maximum curve with 0.25 δ_h are the largest, and those of the maximum curve with 1.0 δ_h are the minimum. The same phenomenon can be found in G9, which need not be repeat here. Generally, for the NSRF

models of SSPs in the deep sliding zone, the change of SOF has a negligible effect on the landslide surface displacement.

4.3 FS analysis

In order to investigate the effects of SSPs uncertainty on landslide stability, the FSs of various models with different time points are analyzed. For the stability analysis of reservoir landslide in a real hydrological year, there are four critical time points [e.g., reservoir water level rising to 175 m (60d), before the reservoir water drawdown (120d), reservoir water level dropped to 145 m (280d), and reservoir water level maintained at 145 m (360d)], which are chosen to calculate the FSs.

The FS results of the NSRF model with 0.25 δ_h are used to analyze the landslide stability at different time points. The distribution characteristics of FSs of four time points are shown in Fig. 14. The FS mean of four points are 1.326, 1.276, 1.215, and 1.247. The FS medians of four points are 1.329, 1.283, 1.230, and 1.232. The FS maximums of four points are 1.462, 1.434, 1.324, and 1.735, And the FS minimums of four points are 1.137, 1.120, 1.015, and 1.004. It can be noted from Fig. 14 that the mean, medians, minimums and maximums of FS decrease for the first three points, and increase at the last point. Further analysis shows that the landslide stability is the worst when the reservoir water level descends to 145 m. And after a stationary phase of reservoir water level, the landslide stability decreases slightly. As the reservoir water level rising to 175 m, the whole stability is the best. After a stable period, the whole landslide stability increases gradually, and the dispersion of data increases.
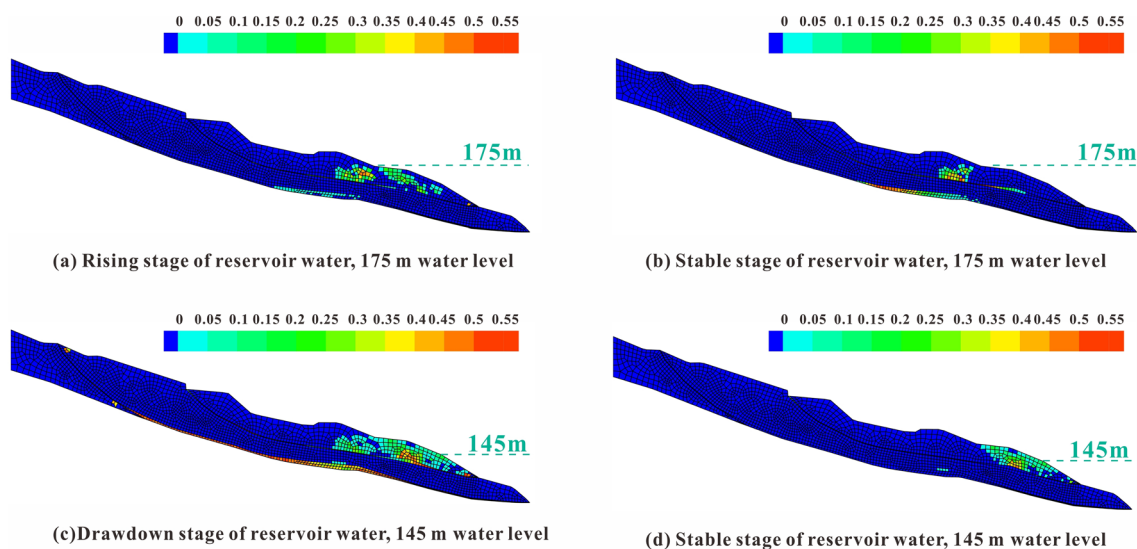

(a) Rising stage of reservoir water, 175 m water level

(b) Stable stage of reservoir water, 175 m water level

(c)Drawdown stage of reservoir water, 145 m water level

(d) Stable stage of reservoir water, 145 m water level

Fig. 15 EFPs of the No. 1 landslide at different time points

In order to study the effect of various NSRF models on the FS of the whole landslide, the 280d point when the stability is worst, is taken as a case. The FS mean of the whole landslide with 0.25 δ_h, 0.5 δ_h, 0.75 δ_h, and 1.0 δ_h are 1.215, 1.211, 1.212, and 1.212. The standard deviations of FSs are 0.040, 0.422, 0.041, and 0.040. It can be seen that the differences of FSs with different SOFs are small.

4.4 EFP analysis

The NSRF model with 0.25 δ_h is taken as an example to investigate the element failure of the No.1 landslide. Figure 15 shows the EFPs of the No.1 landslide at four critical time points. It can be seen that the maximum of EFPs shall not exceed 0.55. As can be seen from Fig. 15a, when the reservoir water level reaches 175 m, the area of element failure mainly distributes in the middle-front part of the shallow landslide. And the element failure in the middle area of the deep sliding zone also occurs, but the EFP of this area is below 0.1. After a 60-day stabilization period (Fig. 15b), we can see that the element failure area is reduced compared with the situation in Fig. 15a, while the values and the area of sliding zones are increasing. This may due to the decrease of the seepage pressure pointed to the landslide, and this can lead to an increase of the residual sliding force. As the reservoir water level drops to 145 m, the element failure area and EFP values increase significantly, as shown in Fig. 15c, the failure area of shallow landslide extends to the toe of the landslide, and the whole area of sliding zones occurs failure. It can also be noted that the EFP values of many elements in the deep sliding zone are more than 0.4, and the EFP values in the front area of the shallow sliding zone are more than 0.35. Then an 80-day stabilization period of reservoir water is carried out, and the result is shown in Fig. 15d. The element failure area and the EFP values decrease remarkably. The failure area almost only occurs in the front part of the shallow landslide. Because the pore pressure perpendicular to the landslide surface is down, and the seepage pressure pointed to the outside of the landslide dissipates.

In summary, the description of the failure area is consistent with the actual deformation situation of the No.1 landslide. Based on the element failure area of different stages, we can have an overall understanding of the deformation and evolutionary process of the No. 1 landslide. It is helpful to guide the mechanism analysis and the control of reservoir landslides.

5 Discussions

5.1 Effect of the uncertainty of SSPs on the landslide deformation and stability

For the consideration of the uncertainty of SSPs of slip soil, the RV model takes the randomness of SSPs into account.
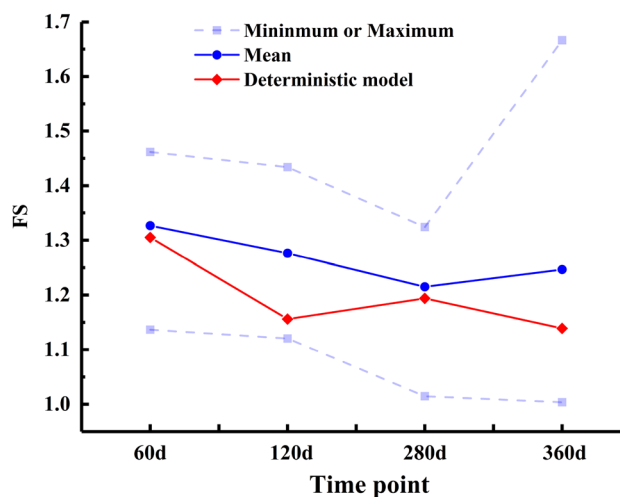

Fig. 16 FSs of the No. 1 landslide at different time points

One value is generated in the whole shallow sliding zone, and the variability of the RV model is big. For the NSRF model, with the application of the SOF, the trend characteristics, and the autocorrelation function, the spatial correlation structures of soil properties can be considered. And the randomness of parameters decreases by considering the trend characteristics. The various SOFs represent different variabilities of soil properties [19]. As the vertical SOF gets larger, the variability of SSPs becomes smaller.

In this study, no significant differences in the landslide surface displacement, EFP and FS are found between various NSRF models of the deep sliding zone. There are probably three chief causes for the results. (1) the fluctuation extent of data depends on the standard deviation of the residual component, and the standard deviation of the residual component is relatively small due to the separation of the trend component, especially when the tendency is dominant. (2) Some characteristic indexes of landslides are not sensitive to the change of SSPs in the deep sliding zone caused by vertical SOF. (3) Compared with the deep sliding mass of No.1 landslide, the shallow sliding mass is the main deformable body under the rainfall and reservoir water condition [3].

During the conventional landslide stability analysis, the actual spatial variability and randomness of soil properties are not considered. And the deterministic analysis in previous studies is not able to obtain some indexes (e.g., statistical indicators, EFP) and extreme cases of a landslide. It is necessary to explore the differences between the deterministic model of current literature and the uncertain models of this paper. The SSPs of sliding zones reported by Ni et al. [34] are adopted in the deterministic model. The FSs of the landslide at four time points are 1.305, 1.156, 1.194, and 1.139. The FSs of the uncertain model (0.25 δ_h) and the deterministic model are plotted in Fig. 16. It can be noted that
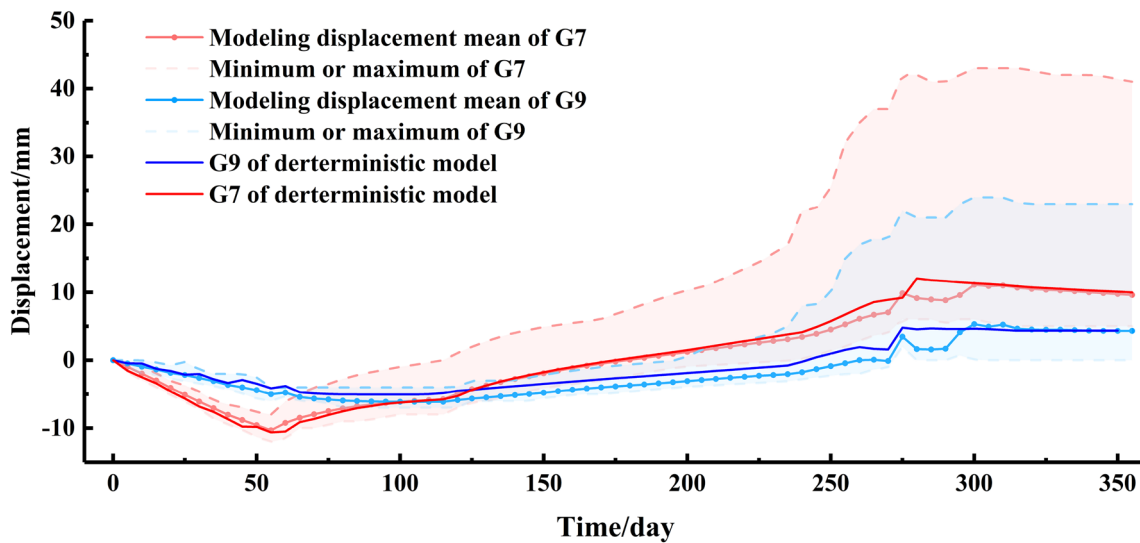
Fig. 17 Landslide surface displacement curves of deterministic model and uncertain model
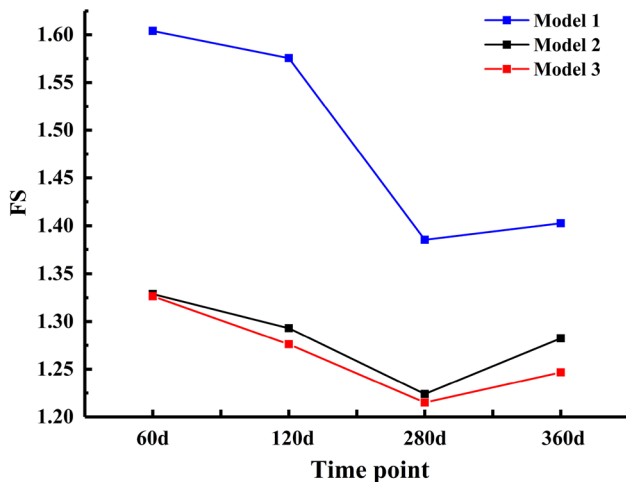

Fig. 18 Mean FSs of three models at different time points

that the FSs of the deterministic model are smaller than the FSs mean of the uncertain model. The time point of the least FS is in 120d for the deterministic model, while that of the least FS is in 280d for the uncertain model. And the FS trend of the deterministic model is different from that of uncertain models. However, the FSs of the deterministic model are still in the range of the FSs extremum of the uncertain model.

The G7 and G9 displacements of the uncertain and deterministic models are drawn in Fig. 17. It can be seen that the displacement curves of the deterministic model are close to the mean displacement curves. And the displacements of the deterministic model are slightly larger than the mean displacements. All in all, considering the actual spatial variability of soil properties, it is great of realistic significance

to establish a random field model and obtain comprehensive results of landslide stability.

5.2 FS estimation with different strength reduction regions

The SRFE method is under the concept of the limit equilibrium slice method. The whole SRFE method is widely used to calculate the FS of slope or landslide in which the sliding zone is not determined. And the local SRFE method is more suitable for the landslide with clear sliding zones [45]. For the common landslide with a single sliding zone, there is no doubt about the strength reduction region, and the FS represents the stability of the whole landslide. However, for the landslide with multi-sliding zones, it is necessary to explore the effect of various strength reduction regions on the FS.

For the No.1 landslide with double-sliding zones, the shallow sliding zone, the deep sliding zone, and two sliding zones are selected respectively as the strength reduction regions to calculate the FSs. Model 1, model 2, and model 3 are used to denote the No.1 landslide connected with those three reduction regions. The NSRF model with 0.25 δ_h is taken as a case. The FSs mean of the three models are plotted in Fig. 18. It can be noted that the FS mean of model 1 is much greater than that of model 2 and model 3. The FS mean of model 2 is slightly larger than that of model 3. The change of strength reduction regions inevitably leads to the change of FS.

With the reduction of SSPs only in the shallow sliding zone, the shallow sliding mass has a large displacement deformation, and the plastic zone gradually runs through the shallow sliding zone, the shallow sliding mass may attain the limit equilibrium state. To some extent, the FS

of model 1 reflects the stability of the shallow sliding mass. For model 2, the plastic zone is expanding along with the reduction of SSPs in the deep sliding zone, the region above the deep sliding zone moves together as a whole. And the FS of model 2 may reflect the stability of the whole sliding mass. Compared with model 1 and model 2, the reduction of SSPs in double sliding zones is considered in model 3. The FS results are more conservative as the reduction area increases. In conclusion, the weakness of SSPs exists in the multi-sliding zones during landslide evolution, the multi-sliding zones should be selected as the reduction area to obtain the FS of the whole landslide.

5.3 Deficiency in this research

1. Due to the limitation of data, the spatial variation of SSPs is not considered for the shallow sliding zone, while the randomness of SSPs is studied using the RV model. And this study focuses on the SSPs of sliding zones, other mechanical parameters are not considered.
2. The few sampling points of sliding zones are not enough to obtain the spatial variation of SSPs in the vertical direction, therefore, the vertical SOFs are assumed to be 0.25, 0.5, 0.75, and 1.0 times of the horizontal SOF. Some NSRF models are then established
3. The effect of other parameters on the numerical software convergence is not studied here, because it is not the purpose of this present study. In this paper, based on the un-convergence mechanism of numerical software, the SSPs are roughly filtered.
4. In order to investigate the deformation and stability of reservoir landslide under real reservoir water operation conditions in TGRA, a real hydrological year is adopted in the fluid–solid numerical simulation, and the extreme operating condition is not considered.
5. All in all, this research aims to study the effect of uncertain variables SSPs with negative correlation characteristics on the deformation and stability of reservoir landslides, and a nonintrusive stochastic finite element program is built. The approach and some meaningful results can provide a reference to other researchers.

6 Conclusions

This paper proposes a comprehensive nonintrusive stochastic finite element procedure for the reservoir landslide uncertain analysis under real simulation conditions. And the RV model and NSRF models involving the negative correlated non-normal variables are built. The spatial variation characteristics of the SSPs in the sliding zones are investigated in detail using the geostatistics-based method, Copula method, and ACF method. In addition, the surface displacement, landslide stability, and EFP are explored. Several conclusions can be learned from this study.

1) The spatial variability of the SSPs of sliding zone soil is an objective fact. And there is an observable trend of SSPs along the sliding direction. The c increases in the sliding direction, while the φ is in decreasing tendency along with the sliding direction. Some important parameters, such as SSPs distribution types, correlation characteristics between c and φ, and the horizontal SOF of SSPs are obtained. It can provide references for the reliability and spatial variability analyses of landslides.
2) With the application of the uncertain models on the landslide stability analysis, the statistical parameters of the response indexes of landslides enable us to have a clearer understanding and profound understanding of landslide deformation and evolution characteristics. Compared with the deterministic analysis, the spatial deformation possibility of a landslide, the displacement change interval, and the overall tendency of stability can also be obtained.
3) For the No. 1 landslide, the front and middle parts of the shallow sliding mass are the main areas of deformation and failure, and when the reservoir water level drops to the lowest, the stability is worst. As to the calculation of the overall landslide stability with multisliding zones, the conservative results can be obtained when the multisliding zones are selected as the reduction areas, and this choice is relatively consistent with the evolution of landslide.

References

1. Tang HM, Wasowski J, Juang CH (2019) Geohazards in the three Gorges Reservoir Area, China-Lessons learned from decades of research. Eng Geol 261:105267–105267
2. Tang HM, Zou ZX, Xiong CR, Wu YP, Hu XL, Wang LQ, Li CD (2015) An evolution model of large consequent bedding rockslides, with particular reference to the Jiweishan rockslide in Southwest China. Eng Geol 186:17–27
3. Tang HM, Li CD, Hu XL, Su AJ, Wang LQ, Wu YP, Criss RE, Xiong CR, Li YA (2015) Evolution characteristics of the Huangtupo landslide based on in situ tunneling and monitoring. Landslides 12(3):511–521
4. Wang JE, Su AJ, Liu QB, Xiang W, Yeh HF, Xiong CR, Zou ZX, Zhong C, Liu JQ, Cao S (2018) Three-dimensional analyses of the sliding surface distribution in the Huangtupo No. 1 riverside

sliding mass in the Three Gorges Reservoir area of China. Landslides 15:1425–1435

5. Cui DS, Wang S, Chen Q, Wu W (2021) Experimental Investigation on Loading-Relaxation Behaviors of Shear-Zone Soil. Int J Geomech 21(4):06021003

6. Wen BP, Aydin A, Duzgoren-Aydin NS, Li YR, Chen HY, Xiao SD (2007) Residual strength of slip zones of large landslides in the Three Gorges area. China Eng Geol 93(3–4):82–98

7. Jiang JW, Xiang W, Rohn J, Zeng W, Schleier M (2015) Research on water–rock (soil) interaction by dynamic tracing method for Huangtupo landslide, Three Gorges Reservoir, PR China. Environ Earth Sci 74(1):557–571

8. Lu S, Tang HM, Zhang YQ, Gong WP, Wang LQ (2018) Effects of the particle-size distribution on the micro and macro behavior of soils: fractal dimension as an indicator of the spatial variability of a slip zone in a landslide. Bull Eng Geol Environ 77(2):665–677

9. Tan QW (2019) Study on the structural capacity of sliding zone soil based on the in-situ triaxial test and its application – taking the Huangtupo landslide as an example. China University of Geoscience (**in Chinese**)

10. Miao FS, Wu YP, Li LW, Tang HM, Xiong F (2020) Weakening laws of slip zone soils during wetting–drying cycles based on fractal theory: a case study in the Three Gorges Reservoir (China). Acta Geotech 15:1909–1923

11. Wen BP, Aydin A (2003) Microstructural study of a natural slip zone: quantification and deformation history. Eng Geol 68(3–4):289–317

12. Zhao LH, Zuo S, Lin YL, Li L, Zhang YB (2016) Reliability back analysis of shear strength parameters of landslide with three-dimensional upper bound limit analysis theory. Landslides 13(4):711–724

13. El-Ramly H, Morgenstern NR, Cruden DM (2002) Probabilistic slope stability analysis for practice. Can Geotech J 39(3):665–683

14. Phoon KK, Kulhawy FH (1999) Characterization of geotechnical variability. Can Geotech J 36(4):612–624

15. Li DQ, Qi XH, Phoon KK, Zhang LM, Zhou CB (2014) Effect of spatially variable shear strength parameters with linearly increasing mean trend on reliability of infinite slopes. Struct Saf 49:45–55

16. Li DQ, Xiao T, Cao ZJ, Phoon KK, Zhou CB (2016) Efficient and consistent reliability analysis of soil slope stability using both limit equilibrium analysis and finite element analysis. Appl Math Model 40(9–10):5216–5229

17. Jiang SH, Li DQ, Zhang LM, Zhou CB (2014) Slope reliability analysis considering spatially variable shear strength parameters using a non-intrusive stochastic finite element method. Eng Geol 168:120–128

18. Huang J, Lyamin AV, Griffiths DV, Krabbenhoft K, Sloan SW (2013) Quantitative risk assessment of landslide by limit analysis and random fields. Comput Geotech 53:60–67

19. Griffiths DV, Huang J, Fenton GA (2015) Probabilistic slope stability analysis using RFEM with non-stationary random fields. In: Schweckendiek T, van Tol F, Pereboom D, van Staveren M, Cools P (eds) Geotechnical safety and risk V. IOS Press, Amsterdam, The Netherlands, pp 704–709

20. Jiang SH, Huang J (2016) Efficient slope reliability analysis at low-probability levels in spatially variable soils. Comput Geotech 75:18–27

21. Jiang SH, Huang JS (2018) Modeling of non-stationary random field of undrained shear strength of soil for slope reliability analysis. Soils Found 58(1):185–198

22. Jiang SH, Liu X, Huang JS (2020) Non-intrusive reliability analysis of unsaturated embankment slopes accounting for spatial variabilities of soil hydraulic and shear strength parameters. Eng Comput. https://doi.org/10.1007/s00366-020-01108-6

23. Jiang SH, Papaioannou I, Straub D (2018) Bayesian updating of slope reliability in spatially variable soils with in-situ measurements. Eng Geol 239:310–320

24. Yang HQ, Zhang LL, Xue JF, Zhang J, Li X (2019) Unsaturated soil slope characterization with karhunen–loève and polynomial chaos via bayesian approach. Eng Comput 35(1):337–350

25. Jiang SH, Huang J, Qi XH, Zhou CB (2020) Efficient probabilistic back analysis of spatially varying soil parameters for slope reliability assessment. Eng Geol 271:105597

26. Wu YP, Cheng C, He GF, Zhang QX (2014) Landslide stability analysis based on random-fuzzy reliability: taking Liangshuijing landslide as a case. Stoch Env Res Risk A 28(7):1723–1732

27. Miao FS, Wu YP, Xie YH, Yu F, Peng LJ (2017) Research on progressive failure process of Baishuihe landslide based on Monte Carlo model. Stoch Env Res Risk A 31(7):1683–1696

28. Tang XS, Li DQ, Rong G, Phoon KK, Zhou CB (2013) Impact of copula selection on geotechnical reliability under incomplete probability information. Comput Geotech 49:264–278

29. Tang XS, Li DQ, Zhou CB, Phoon KK (2015) Copula-based approaches for evaluating slope reliability under incomplete probability information. Struct Saf 52:90–99

30. Li C, Tang HM, Han DW, Zou ZX (2019) Exploration of the creep properties of undisturbed shear zone soil of the Huangtupo landslide. Bull Eng Geol Environ 78(2):1237–1248

31. Li B, Tang HM, Gong WP, Tan QW, Zhang GC (2018) Stability analysis of sliding mass I at riverside of Huangtupo landslide in one hydrological year. J Eng Geol 26(s1):167–173 (**in Chinese**)

32. O'Connor AJ, Kenshel O (2012) Experimental evaluation of the scale of fluctuation for spatial variability modeling of chloride-induced reinforced concrete corrosion. J Bridge Eng 18(1):3–14

33. Onyejekwe S, Kang X, Ge L (2016) Evaluation of the scale of fluctuation of geotechnical parameters by autocorrelation function and semivariogram function. Eng Geol 214:43–49

34. Ni WD, Tang HM, Hu XL, Wu YP, Su AJ (2013) Research on deformation and stability evolution law of huangtupo riverside slump-mass No. 1. Rock Soil Mech 34(10):2961–2970 (**in Chinese**)

35. HIGH (2002) Detailed investigation report of Huangtupo landslide in Badong County, Hubei. Hubei Institute of Geological Hazard, Jingzhou (**in Chinese**)

36. CISPD (2009) Detailed investigation report of Huangtupo landslide in Badong County, Hubei. Changjiang Institute of Survey, Planning, Design (**in Chinese**)

37. Hua S (2015) Genetic mechanism of multi-stages sliding and evolution law of the Huangtupo landslide in the Three Gorges Reservoir Area. China University of Geoscience (**in Chinese**)

38. Luo C, Yin KL, Chen LX, Jian WX (2005) Probability distribution fittingand optimization of shear strength parameters in sliding zone along horizontal-stratum landslides in wanzhou city. Chin J Rock Mech Eng 24(9):1588–1593 (**in Chinese**)

39. Li YY, Yin KL, Chai B, Zhang GR (2008) Study on statistical rule of shear strength parameters of soil in landslide zone in three gorges reservoir area. Rock Soil Mech 29(5):1419–1418 (**in Chinese**)

40. Gundogdu KS, Guney I (2007) Spatial analyses of groundwater levels using universal kriging. J Earth Syst Sci 116(1):49–55

41. Brus DJ, Heuvelink GB (2007) Optimization of sample patterns for universal kriging of environmental variables. Geoderma 138(1–2):86–95

42. Xue Y, Wu YP, Miao FS, Li LW, Liao K, Ou GZ (2020) Effect of spatially variable saturated hydraulic conductivity with non-stationary characteristics on the stability of reservoir landslides. Stoch Env Res Risk A 34(2):311–329

43. Zheng YR, Zhao SY (2004) Application of strength reduction FEM in soil and rock slope. Chin J Rock Mech Eng 23(19):3381–3388 (**in Chinese**)

44. Huang MS, Jia CQ (2009) Strength reduction FEM in stability analysis of soil slopes subjected to transient unsaturated seepage. Comput Geotech 36(1–2):93–101

45. Yang GH, Zhong ZH, Fu XD, Zhang YC, Wen Y, Zhang MF (2014) Slope analysis based on local strength reduction method and variable–modulus elasto-plastic model. J Cent South Univ 21:2041–2050

Publisher's Note Springer Nature remains neutral with regard to jurisdictional claims in published maps and institutional affiliations.